ISSN 1064-2269, Journal of Communications Technology and Electronics, 2014, Vol. 59, No. 12, pp. 1451–1464. © Pleiades Publishing, Inc., 2014.
Original Russian Text © J.L. López-Martínez, V.I. Kober, V.N. Karnaukhov, 2014, published in Informatsionnye Protsessy, 2014, Vol. 14, No. 1, pp. 87–107.

MATHEMATICAL MODELS, COMPUTATIONAL METHODS

Image Restoration with a Microscanning Imaging System

J. L. López-Martínez[a], V. I. Kober[b, c], and V. N. Karnaukhov[c]

[a] *School of Mathematics, Autonomous University of Yucatan, 97000 Merida, YUC, Mexico*
[b] *Department of Computer Science, CICESE, Carretera Ensenada-Tijuana 3918, Zona Playitas, Ensenada B.C. 22860, Mexico*
[c] *Institute for Information Transmission Problems, Russian Academy of Sciences, Bol'shoi Karetnyi per. 19, str. 1, Moscow, 127994 Russia*
e-mail: vnk@iitp.ru

Received February 1, 2014

Abstract—Traditional methods of image restoration use only one observed image for processing. In this paper, we propose methods for image restoration using several distorted images obtained with a microscanning imaging system. We assume that the observed images contain an original image degraded either by additive or by multiplicative interferences. Additionally, the images are corrupted with the additive noise of a receiver sensor. Using a set of observed images, image restoration is carried out by solving a system of equations that is derived from optimization of an objective function. Since the proposed restoration methods possess a high computational complexity, a fast algorithm is proposed. Computer simulation results obtained with the proposed methods are analyzed in terms of restoration accuracy, tolerance to the additive input noise, and robustness to sensors'position errors.

Keywords: image restoration, image processing, microscanning
DOI: 10.1134/S1064226914120122

INTRODUCTION

Image restoration is an important subject of research in image processing, because its methods and technologies can be applied for restoration of images corrupted due to the imperfectness of the imaging process [1]. There is a wide class of distortions [2, 3], such as motion aberrations [2, 3], geometrical distortions, nonuniform scene illumination, influence of the environment (fog, clouds, etc.) [4, 6], noise (impulse noise, white noise, etc.), and errors of sensors in imaging systems. For example, focal-plane array sensors are subject to additive distortions [7]. These distortions are spatially nonuniform and arise from the difference between the characteristics of individual sensors in the array [8]. An example of multiplicative interferences is the kind of distortions arising from nonuniform scene illumination [9]. In this paper, we will consider two types of interferences: additive and multiplicative. Most existing methods of image restoration use only one observed image [10–12]. Recently, an algorithm was proposed for restoration of additive distortions with the use of three observed images obtained by means of microscanning [13–16]. Microscanning is a technique of time-sequential input of the same scene with a small displacement of the camera relative to the observed scene [17]. This technique can be applied to image restoration problems only if the initial image signal and interferences can be mutually displaced in space in a series of observed images obtained with the use of microscanning. Microscanning can be performed by means of controlled displacements of the camera or by controlled displacements of the light source (in the problem of elimination of the nonuniformity of illumination). In this study, we use five observed images obtained by means of isotropic microscanning. For this case, a system of linear equations is obtained. Since the computational complexity of the method is high, a fast algorithm enabling one to restore images with a high speed is proposed. The accuracy of image reconstruction in the cases of nonuniform illumination and a strong additive interference is estimated.

The structure of the paper is the following. Section 1 presents the methods for image restoration from additive and multiplicative interferences. In Section 2, a fast algorithm for image restoration is described. Results of computer simulation are presented in Section 3. Our conclusions are presented in the end of this paper.

1. METHODS OF IMAGE RESTORATION

Let us introduce some useful notations and definitions. We assume that $\{s_t(k, l), t = 1, 2, ..., T\}$ is the observed image, where t is the index of the image in a time sequence recorded in the process of microscanning, T is the number of observed images (3 or 5), and (k, l) are the pixel coordinates. Without loss of gener-

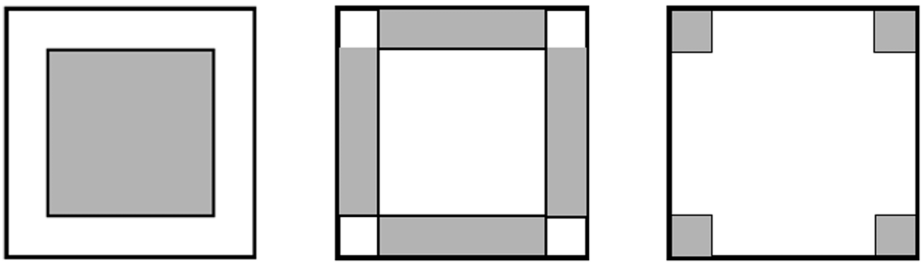

Fig. 1. Spatial support regions of functions used for construction of the objective functions: (a) central part, (b) boundary elements except for corner elements, and (c) corner elements.

ality, we can assume that each image has a size of $M \times M$ pixels, where $M = 2^m$ and m is a positive integer number. Let $\{f(k, l)\}$, $\{b(k, l\}$, and $\{a(k, l)\}$ denote the initial image, the additive interference, and the multiplicative interference, respectively. Assume that these images are time-invariant during the capture procedure. Let $\{n_t(k, l)\}$ be a time-varying Gaussian white noise with zero mean. Since the model of distortion with five observed images involves the model with three images, we assume that $T = 5$.

1.1. Additive Model of Distortion

If the image is distorted by an inhomogeneous additive interference, the observed scene can be described as

$$s_1(k, l) = b(k, l) + f(k, l) + n_1(k, l),$$
$$1 \le k \le M, \quad 1 \le l \le M.$$

By means of microscanning, four successive frames with vertical and horizontal displacements by one pixel are obtained as

$$s_2(k, l) = b(k-1, l) + f(k, l) + n_2(k, l),$$
$$1 \le k \le M, \quad 1 \le l \le M,$$
$$s_3(k, l) = b(k, l-1) + f(k, l) + n_3(k, l),$$
$$1 \le k \le M, \quad 1 \le l \le M,$$
$$s_4(k, l) = b(k+1, l) + f(k, l) + n_4(k, l),$$
$$1 \le k \le M, \quad 1 \le l \le M,$$
$$s_5(k, l) = b(k, l+1) + f(k, l) + n_5(k, l),$$
$$1 \le k \le M, \quad 1 \le l \le M.$$

Using these expressions, let us calculate matrices R_1 and R_2 of the vertical gradient and matrices C_1 and C_2 of the horizontal gradient. First of all, we set the boundary elements of the matrices to zero as follows:

$$R_1(M, l) = 0, \quad R_2(k, 1) = 0, \quad C_1(M, l) = 0,$$
$$C_1(k, 1) = 0, \quad 1 \le k \le M, \quad 1 \le l \le M.$$

The remaining elements of the matrix are calculated as follows:

$$R_1(k, l) = s_1(k, l) - s_2(k+1, l)$$
$$= f(k, l) - f(k+1, l) + n_1(k, l) - n_2(k+1, l),$$
$$1 \le k \le M, \quad 1 \le l \le M;$$
$$R_2(k, l) = s_1(k, l) - s_4(k-1, l)$$
$$= f(k, l) - f(k-1, l) + n_1(k, l) - n_4(k-1, l),$$
$$1 \le k \le M, \quad 1 \le l \le M;$$
$$C_1(k, l) = s_1(k, l) - s_3(k, l+1)$$
$$= f(k, l) - f(k, l+1) + n_1(k, l) - n_3(k, l+1),$$
$$1 \le k \le M, \quad 1 \le l \le M;$$
$$C_2(k, l) = s_1(k, l) - s_5(k, l-1)$$
$$= f(k, l) - f(k, l-1) + n_1(k, l) - n_5(k, l-1),$$
$$1 \le k \le M, \quad 1 \le l \le M.$$

Then we want to minimize the variance of the additive noise contained in these matrices. The objective function to be minimized can be written as follows:

$$F^A = F_a^A + F_b^A + F_c^A, \tag{1}$$

where F_a^A, F_b^A, and F_c^A define the regions of supports of these functions. These regions are shown in Fig. 1. In expression (1), F_a^A contains information on the noise in the central part of the image without regard to the boundaries, i.e.,

$$F_a^A = \sum_{k=2}^{M-1} \sum_{l=2}^{M-1} ([R_1(k, l) - f(k, l) + f(k+1, l)]^2$$
$$+ [C_1(k, l) - f(k, l) + f(k, l+1)]^2 + [R_2(k, l) - f(k, l)$$
$$+ f(k-1, l)]^2 + [C_2(k, l) - f(k, l) + f(k, l-1)]^2). \tag{2}$$

F_b^A contains information on the noise along the boundaries of the image without regard to the corner elements,

$$F_b^A = \sum_{l=2}^{M-1}([R_1(1,l)-f(1,l)+f(2,l)]^2+[C_1(1,l)-f(1,l)+f(1,l+1)]^2+[C_2(1,l)-f(1,l)+f(1,l-1)]^2)+\sum_{k=2}^{M-1}([R_1(k,M)-f(k,M)+f(k+1,M)]^2+[R_2(k,M)-f(k,M)+f(k-1,M)]^2+[C_2(k,M)-f(k,M)+f(k,M-1)]^2)+\sum_{l=2}^{M-1}([C_1(M,l)-f(M,l)+f(M,l+1)]^2+[R_2(M,l)-f(M,l)+f(M-1,l)]^2+[C_2(M,l)-f(M,l)+f(M,l-1)]^2)+\sum_{k=2}^{M-1}([R_1(k,1)-f(k,1)+f(k+1,1)]^2+[C_1(k,1)-f(k,1)+f(k,2)]^2+[R_2(k,1)-f(k,1)+f(k-1,1)]^2). \quad (3)$$

F_c^A is based on the information on the noise at four corner points of the image:

$$F_c^A = [R_1(1,1)-f(1,1)+f(2,1)]^2+[C_1(1,1)-f(1,1)+f(1,2)]^2+[R_1(1,M)-f(1,M)+f(2,M)]^2+[C_2(1,M)-f(1,M)+f(1,M-1)]^2+[R_2(M,M)-f(M,M)+f(M-1,M)]^2+[C_2(M,M)-f(M,M)-f(M,M-1)]^2+[C_1(M,1)-f(M,1)+f(M,2)]^2+[R_2(M,1)-f(M,1)+f(M-1,1)]^2. \quad (4)$$

Minimization of objective function (1) with respect to $f(k, l)$ leads to a system of linear equations, which can be written in the matrix form as

$$\mathbf{Af} = \mathbf{u},$$

where $\mathbf{A}$ is the $M^2 \times M^2$ matrix, $\mathbf{f}$ is the vector version of the initial image with dimensions $M^2 \times 1$, and vector $\mathbf{u}$ is defined as

$$\mathbf{u} = \mathbf{u}_R + \mathbf{u}_C,$$

and its size is $M^2 \times 1$. Vectors $\mathbf{u}_R$ and $\mathbf{u}_C$ are calculated as follows:

$$\mathbf{u}_R(l) = R_1(1,l) - R_2(2,l), \quad \text{for } 1 \le l \le M,$$

$$\mathbf{u}_R(kM+l) = R_1(k+1,l) - R_1(k,l) + R_2(k+1,l) - R_2(k+2,l), \quad \text{for } 1 \le l \le M, \quad 1 \le k \le M-2,$$

$$\mathbf{u}_R(M^2-l) = -R_1(M-1,M-l) + R_2(M,M-l), \quad \text{for } 0 \le l \le M-1,$$

$$\mathbf{u}_C(kM+1) = -C_1(k+1,1) + C_2(k+1,2), \quad \text{for } 0 \le k \le M-1,$$

$$\mathbf{u}_C(kM+l) = -C_1(k+1,1) - C_1(k+1,l-1) + C_2(k+1,l) - C_2(k+1,l+1), \quad \text{for } 2 \le l \le M-1, \quad 0 \le k \le M-1,$$

$$\mathbf{u}_C(k) = -C_1(k,M-1) + C_2(k,M), \quad \text{for } 0 \le k \le M-1.$$

Matrix $\mathbf{A}$ is sparse and its nonzero elements can be represented as

$$\mathbf{A} = \begin{bmatrix} \mathbf{A}_1 & \mathbf{A}_3 & 0 & 0 & 0 & 0 \\ \mathbf{A}_3 & \mathbf{A}_2 & \mathbf{A}_3 & 0 & 0 & 0 \\ 0 & \mathbf{A}_3 & \mathbf{A}_2 & \mathbf{A}_3 & 0 & 0 \\ 0 & 0 & \ddots & \ddots & \ddots & 0 \\ 0 & 0 & 0 & \mathbf{A}_3 & \mathbf{A}_2 & \mathbf{A}_3 \\ 0 & 0 & 0 & 0 & \mathbf{A}_3 & \mathbf{A}_1 \end{bmatrix},$$

where matrices $\mathbf{A}_1$, $\mathbf{A}_2$, and $\mathbf{A}_3$ can be written in the explicit form as

$$\mathbf{A}_1 = \begin{bmatrix} 2 & -1 & 0 & 0 & 0 & 0 \\ -1 & 3 & -1 & 0 & 0 & 0 \\ 0 & -1 & 3 & -1 & 0 & 0 \\ 0 & 0 & \ddots & \ddots & \ddots & 0 \\ 0 & 0 & 0 & -1 & 3 & -1 \\ 0 & 0 & 0 & 0 & -1 & 2 \end{bmatrix},$$

$$\mathbf{A}_2 = \begin{bmatrix} 3 & -1 & 0 & 0 & 0 & 0 \\ -1 & 4 & -1 & 0 & 0 & 0 \\ 0 & -1 & 4 & -1 & 0 & 0 \\ 0 & 0 & \ddots & \ddots & \ddots & 0 \\ 0 & 0 & 0 & -1 & 4 & -1 \\ 0 & 0 & 0 & 0 & -1 & 3 \end{bmatrix},$$

$$\mathbf{A}_3 = \operatorname{diag}[-1, -1, \ldots, -1].$$

The rank of the matrix $\mathbf{A}$ is $M^2 - 1$; therefore, the initial image can be restored if one pixel of the image will be preliminary set to a certain constant, e.g., the last pixel will be set to zero. After restoration, the obtained image is processes pointwise so that the mean value is equal to the mean of the initial image. For solving the system of equations, we use the efficient conjugate gradient method [18]. The computational complexity of the method is determined by the order of calculation of the conjugate gradient and the size of the restored image. The complexity is estimated as $O(np)$ operations, where p is the number of nonzero ele-

ments of the matrix and n is the number of iterations needed for solving the system of equations. In our case, $p = O(5M^2)$ and $n = qM$, where q depends on the solution accuracy and $Q \in [3, 10]$ in the conducted experiments. Therefore, the computational complexity of the method can be estimated as $O(5qM^3)$ operations.

1.2. Multiplicative Model of Distortion

If the image is distorted by a multiplicative interference, the model of the image can be expressed as

$$s_1(k, l) = a(k, l)f(k, l) + n_1(k, l),$$
$$1 \le k \le M, \quad 1 \le l \le M,$$

where initial image $\{f(k, l)\}$ is distorted by a multiplicative interference $\{a(k, l)\}$ and additionally distorted by a time-varying additive noise $\{n_1(k, l)\}$. Assuming that microscanning is capable of distinguishing the initial image from the interference, we can obtain several frames of the observed scene, slightly displaced with respect to the original image, in the following form:

$$s_2(k, l) = a(k-1, l)f(k, l) + n_2(k, l),$$
$$1 \le k \le M, \quad 1 \le l \le M,$$
$$s_3(k, l) = a(k, l-1)f(k, l) + n_3(k, l),$$
$$1 \le k \le M, \quad 1 \le l \le M,$$
$$s_4(k, l) = a(k+1, l)f(k, l) + n_4(k, l),$$
$$1 \le k \le M, \quad 1 \le l \le M,$$
$$s_5(k, l) = a(k, l+1)f(k, l) + n_5(k, l),$$
$$1 \le k \le M, \quad 1 \le l \le M.$$

Now we can define four partial matrices using the relations between the rows and columns of the observed images. First of all, we set the boundary elements of the matrices to 1 as follows:

$$V_1(M, l) = 1, \quad V_2(1, l) = 1, \quad H_1(k, M) = 1,$$
$$H_2(k, 1) = 1, \quad 1 \le k \le M, \quad 1 \le l \le M.$$

The remaining elements of the matrix are calculated as follows:

$$V_1(k, l) = \frac{s_1(k, l)}{s_2(k+1, l)}, \quad 1 \le k \le M, \quad 1 \le l \le M; \quad (5)$$

$$V_2(k, l) = \frac{s_1(k, l)}{s_4(k-1, l)}, \quad 1 \le k \le M, \quad 1 \le l \le M; \quad (6)$$

$$H_1(k, l) = \frac{s_1(k, l)}{s_3(k, l+1)}, \quad 1 \le k \le M, \quad 1 \le l \le M; \quad (7)$$

$$H_2(k, l) = \frac{s_1(k, l)}{s_5(k, l-1)}, \quad 1 \le k \le M, \quad 1 \le l \le M. \quad (8)$$

We can see that the multiplicative interference in the matrices is eliminated if the observed image does not contain an additive noise. Therefore, for small fluctuations of the additive noise, matrices in Eqs. (5)–(8) are close to the corresponding partial matrices constructed on the basis of the initial image and its displaced versions. Taking into account properties of the logarithmic function (monotonicity and $\ln(x/y) = \ln(x) - \ln(y)$, let us introduce the following objective function:

$$F^M = F_a^M + F_b^M + F_c^M,$$

where the support regions of functions F_a^M, F_b^M, and F_c^M are the same as for additive model (1)–(4). These functions are defined as follows:

$$F_a^M = \sum_{k=2}^{M-1}\sum_{l=2}^{M-1}([\ln(V_1(k, l)) - \ln(f(k, l))$$
$$+ \ln(f(k+1, l))]^2 + [\ln(H_1(k, l)) - \ln(f(k, l))$$
$$+ \ln(f(k, l+1))]^2 + [\ln(V_2(k, l)) - \ln(f(k, l))$$
$$+ \ln(f(k-1, l))]^2 + [\ln(H_2(k, l)) - \ln(f(k, l))$$
$$+ \ln(f(k, l-1))]^2).$$

$$F_b^M = \sum_{l=2}^{M-1}([\ln(V_1(1, l)) - \ln(f(1, l)) + \ln(f(2, l))]^2$$
$$+ [\ln(H_1(1, l)) - \ln(f(1, l)) + \ln(f(1, l+1))]^2$$
$$+ [\ln(H_2(1, l)) - \ln(f(1, l)) + \ln(f(1, l-1))]^2)$$
$$+ \sum_{k=2}^{M-1}([\ln(V_1(k, 1)) - \ln(f(k, 1)) + \ln(f(k+1, 1))]^2$$
$$+ [\ln(H_1(k, 1)) - \ln(f(k, 1)) + \ln(f(k, 2))]^2$$
$$+ [\ln(V_2(k, 1)) - \ln(f(k, 1)) + \ln(f(k-1, 1))]^2)$$
$$+ \sum_{k=2}^{M-1}([\ln(V_1(k, M)) - \ln(f(k, M)) + \ln(f(k+1, M))]^2$$
$$+ [\ln(V_2(k, M)) - \ln(f(k, M)) + \ln(f(k-1, M))]^2$$
$$+ [\ln(H_2(k, M)) - \ln(f(k, M)) + \ln(f(k, M-1))]^2)$$
$$+ \sum_{l=2}^{M-1}([\ln(H_1(M, l)) - \ln(f(M, l)) + \ln(f(M, l+1))]^2$$
$$+ [\ln(V_2(M, l)) - \ln(f(M, l)) + \ln(f(M-1, l))]^2$$
$$+ [\ln(H_2(M, l)) - \ln(f(M, l)) + \ln(f(M, l-1))]^2).$$

$$F_c^M = [\ln(V_1(1, 1)) - \ln(f(1, 1)) + \ln(f(2, 1))]^2$$
$$+ [\ln(H_1(1, 1)) - \ln(f(1, 1)) + \ln(f(1, 2))]^2$$
$$+ [\ln(V_1(1, M)) - \ln(f(1, M)) + \ln(f(2, M))]^2$$

$$+ [\ln(H_2(1, M)) - \ln(f(1, M)) + \ln(f(1, M-1))]^2$$
$$+ [\ln(V_2(M, M)) - \ln(f(M, M)) + \ln(f(M-1, M))]^2$$
$$+ [\ln(H_2(M, M)) - \ln(f(M, M)) + \ln(f(M, M-1))]^2$$
$$+ [\ln(H_1(M, 1)) - \ln(f(M, 1)) + \ln(f(M, 2))]^2$$
$$+ [\ln(V_2(M, 1)) - \ln(f(M, 1)) + \ln(f(M-1, 1))]^2.$$

2. FAST RESTORATION ALGORITHM

Since the computational complexity of the method proposed is high, we developed a fast restoration algorithm. The idea of this algorithm is the following: let us perform a pyramidal decomposition of the observed images to images of smaller sizes, apply the algorithms to all smaller images, and then reconstruct the restored image from the smaller restored images. For $T = 5$, the pyramidal decomposition of the observed $M \times M$ image $s_1(k, l)$ leads to four smaller images with dimensions $M/2 \times M/2$, which are obtained from the observed image by decimation over even and odd indices along each coordinate. Figure 2 shows an example of the decomposition of the image for $M = 4$ into four smaller images with sizes of 2×2 pixels.

Moreover, for each smaller image, we can form its four shifted versions from the parent larger-size image (as if by simulating the microscanning process on this level of pyramidal decomposition). Repeating this decomposition process, we can obtain the complete pyramidal set of images. It should be noted that this set enables one to restore larger images from smaller images at any level of decomposition.

Let $d = 1, ..., \log(M) - 1$ be the level of pyramidal decomposition and $\{s_t^0(k, l) \equiv s_t(k, l),\ t = 1, 2, ..., T\}$ be some set of observed images. The number of sets of observed images at the dth level of the pyramid is 4^d. Decomposition of a set of observed images into four sets of small observed images at level d is performed as follows:

$$\begin{aligned} s_1^d(k, l; 1) &= s_1^{d-1}(2k-1, 2l-1), \\ s_1^d(k, l; 2) &= s_1^{d-1}(2k, 2l-1), \\ s_1^d(k, l; 3) &= s_1^{d-1}(2k-1, 2l), \\ s_1^d(k, l; 4) &= s_1^{d-1}(2k, 2l), \end{aligned} \tag{9}$$

for $1 \le k \le \frac{M}{2^d},\ 1 \le l \le \frac{M}{2^d}$,

$$\begin{aligned} s_2^d(k, l; 1) &= s_2^{d-1}(2k-1, 2l-1) + s_2^{d-1}(2k-2, 2l-1) \\ &\quad - s_1^{d-1}(2k-2, 2l-1), \\ s_2^d(k, l; 2) &= s_2^{d-1}(2k, 2l-1) + s_2^{d-1}(2k-1, 2l-1) \\ &\quad - s_1^{d-1}(2k-2, 2l-1), \end{aligned}$$

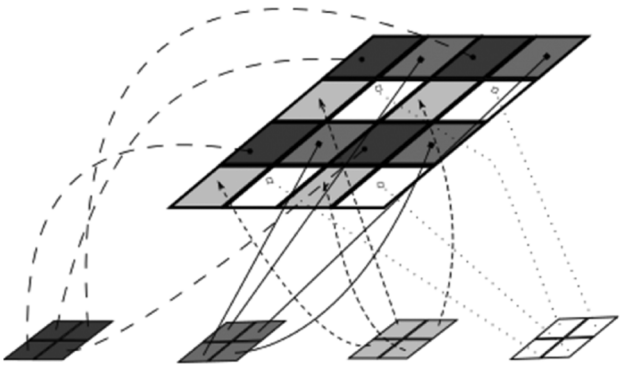

Fig. 2. Illustration of the pyramidal decomposition of the observed image for $M = 4$.

$$\begin{aligned} s_2^d(k, l; 3) &= s_2^{d-1}(2k-1, 2l) + s_2^{d-1}(2k-2, 2l) \\ &\quad - s_1^{d-1}(2k-2, 2l), \\ s_2^d(k, l; 4) &= s_2^{d-1}(2k, 2l) + s_2^{d-1}(2k-1, 2l) \\ &\quad - s_1^{d-1}(2k-1, 2l) \end{aligned} \tag{10}$$

for $1 \le k \le \frac{M}{2^d},\ 1 \le l \le \frac{M}{2^d}$,

$$\begin{aligned} s_3^d(k, l; 1) &= s_3^{d-1}(2k-1, 2l-1) + s_3^{d-1}(2k-1, 2l-2) \\ &\quad - s_1^{d-1}(2k-1, 2l-2), \\ s_3^d(k, l; 2) &= s_3^{d-1}(2k, 2l-1) + s_3^{d-1}(2k, 2l-2) \\ &\quad - s_1^{d-1}(2k, 2l-2), \\ s_3^d(k, l; 3) &= s_3^{d-1}(2k-1, 2l) + s_3^{d-1}(2k-1, 2l-1) \\ &\quad - s_1^{d-1}(2k-1, 2l-1), \\ s_3^d(k, l; 4) &= s_3^{d-1}(2k, 2l) + s_3^{d-1}(2k, 2l-1) \\ &\quad - s_1^{d-1}(2k, 2l-1) \end{aligned} \tag{11}$$

for $1 \le k \le \frac{M}{2^d},\ 1 \le l \le \frac{M}{2^d}$,

$$\begin{aligned} s_4^d(k, l; 1) &= s_4^{d-1}(2k-1, 2l-1) + s_4^{d-1}(2k, 2l-1) \\ &\quad - s_1^{d-1}(2k, 2l-1), \\ s_4^d(k, l; 2) &= s_3^{d-1}(2k, 2l-1) + s_4^{d-1}(2k+1, 2l-1) \\ &\quad - s_1^{d-1}(2k+1, 2l-1), \\ s_4^d(k, l; 3) &= s_4^{d-1}(2k-1, 2l) + s_4^{d-1}(2k, 2l) \\ &\quad - s_1^{d-1}(2k, 2l), \\ s_4^d(k, l; 4) &= s_4^{d-1}(2k, 2l) + s_4^{d-1}(2k+1, 2l) \\ &\quad - s_1^{d-1}(2k+1, 2l) \end{aligned} \tag{12}$$

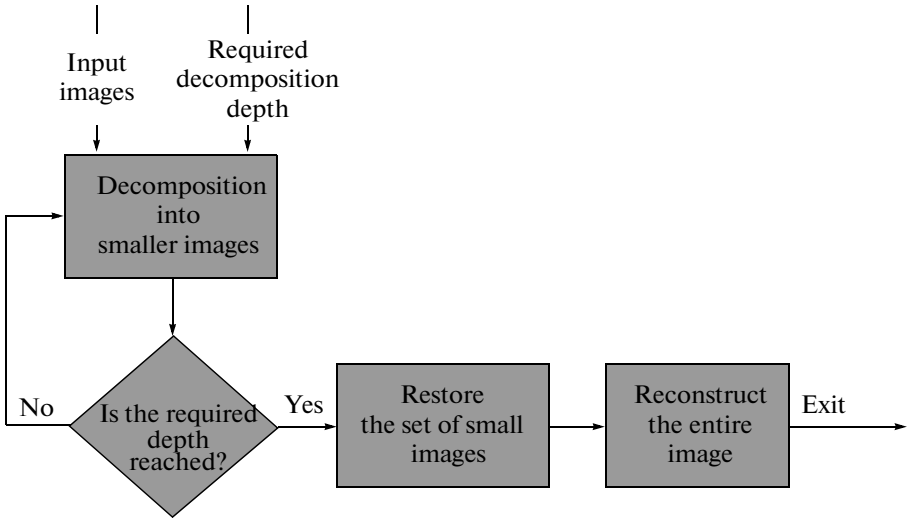

Fig. 3. Flow chart of the fast restoration algorithm.

$$\text{for } 1 \le k \le \frac{M}{2^d},\ 1 \le l \le \frac{M}{2^d},$$

$$\begin{aligned}
s_5^d(k, l; 1) &= s_5^{d-1}(2k-1, 2l-1) + s_5^{d-1}(2k-1, 2l) \\
&\quad - s_1^{d-1}(2k-1, 2l), \\
s_5^d(k, l; 2) &= s_5^{d-1}(2k, 2l-1) + s_5^{d-1}(2k, 2l) \\
&\quad - s_1^{d-1}(2k, 2l), \\
s_5^d(k, l; 3) &= s_5^{d-1}(2k-1, 2l) + s_5^{d-1}(2k-1, 2l+1) \\
&\quad - s_1^{d-1}(2k-1, 2l+1), \\
s_5^d(k, l; 4) &= s_5^{d-1}(2k, 2l) + s_5^{d-1}(2k, 2l+1) \\
&\quad - s_1^{d-1}(2k, 2l+1)
\end{aligned} \tag{13}$$

$$\text{for } 1 \le k \le \frac{M}{2^d},\ 1 \le l \le \frac{M}{2^d}.$$

The flow chart of the fast restoration algorithm is presented in Fig. 3. The algorithm consists of the following steps:

1. Specify the desired level of pyramidal decomposition.

2. Decompose input images into smaller images according to expressions (9)–(13).

3. If the desired level of decomposition is reached, then go to step 4 else go to step 2.

4. Restore smaller images by the conjugate gradient method.

5. Reconstruct the restored image from the set of smaller images obtained in step 4.

The computational complexity of the algorithm is determined mainly by the complexity of the conjugate gradient method at a given level of decomposition, which can be estimated as $O\left(5Q\frac{M^3}{2^d}\right)$. Additional expenditures stem from the pyramidal decomposition process and the process of reconstruction of the initial image from small images.

3. COMPUTER SIMULATION

In this section, we analyze the quality of restoration by the proposed methods in terms of the root-mean-square error (RMSE), the visual criterion of quality, and the robustness to the position errors of the matrix receiver. The RMSE is defined as

$$\text{RMSE} = \sqrt{\frac{\sum_{k,l}^{M} (f(k, l) - \tilde{f}(k, l))^2}{M^2}},$$

where $\{f(k, l)\}$ and $\{\tilde{f}(k, l)\}$ are the original and restored images, respectively. The size of the images used in our experiments was 256 × 256 pixels, and the signal range was [0, 255]. All experiments were conducted on a computer with Intel Core 2 Duo processor (frequency 2.26 GHz, 2 GB RAM). In order to guarantee statistically correct results, each experiment was repeated 30 times with different realizations of the input noise. The conjugate gradient iterative method was used for solving the systems of linear equations with the following termination condition: the maximum deviation of the signal at the current step from the signal at the previous step is no more than 10^{-10}. The visual criterion was the enhanced difference between the initial and final images [19]:

$$\text{EDIF}(k, l) = c_1(f(k, l) - \tilde{f}(k, l)) + c_2,$$

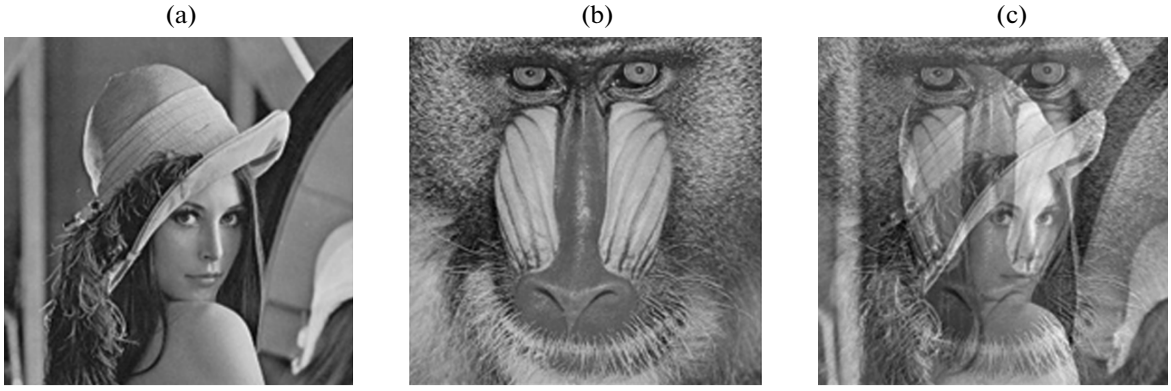

Fig. 4. (a) Original image, (b) inhomogeneous additive interference, and (c) observed image distorted by the inhomogeneous additive interference and a white noise with a standard deviation of 2.

where c_1 and c_2 are normalization constants, which take in our experiments the values $c_1 = 4$ and $c_2 = 128$ in the additive model and $c_1 = 1$ and $c_2 = 128$ in the multiplicative model. If, at a certain point, the error of restoration is zero, the corresponding enhanced difference is represented by gray color defined by constant c_2. Maximum errors are represented in the enhanced difference image by either black or white color (the values of 0 or 255, respectively).

One of the most popular methods of restoration is the linear optimal filtering with the quadratic criterion. However, this method is applicable only to spatially homogeneous (stationary) signals. In these conditions, an appropriate method is the Wiener filtering [3]. The frequency characteristic of an empiric Wiener filter in the presence of only an additive interference is written as

$$H_{\mathrm{w}}(\omega) = \frac{P_S(\omega) - P_N(\omega)}{P_S(\omega)},$$

where $P_S(\omega)$ is the spectral density of the observed distorted scene and $P_N(\omega)$ is the spectral density of the additive interference. This filter was synthesized with known parameters of distortions, which, strictly speaking, overestimates the real ability of restoration with the use of this method. It should be noted that the methods proposed do not use information on distortions. In the case of the multiplicative model, we first performed elementwise logarithmation of the observed image, ignoring the additive noise. Therefore, the multiplicative model turns into the additive model. The transformed signal was subject to the Wiener filtering and the result was subject to the elementwise exponentiation.

3.1. Additive Inhomogeneous Interferences

Figures 4a–4c illustrate the original test image, the image of the inhomogeneous interference, and the distorted image additionally degraded by white Gaussian noise with zero mean and a standard deviation (STD) of 2. The mean and the STD of the interference are 130 and 40, respectively. Figures 5a and 5c show images restored with the use of three and five observed images, respectively. Figures 5b and 5d show the enhanced difference between the original image and the images restored with the use of three and five observed images, respectively. As was expected, isotropic microscanning with five images provides better quality of restoration. Figure 6 shows the results of reconstruction with respect to the RMSE for three observed images (Am3), for five observed images (Am5), and for the Wiener filtering versus the STD of the additive input noise. It should be noted that the restoration algorithms proposed in this paper restore the image significantly better than the Wiener filter with known parameters. This is also explained by the fact that additive interferences are not spatially homogeneous and, therefore, application of the Wiener filter to this model is incorrect. Table 1 presents the results of restoration with the use of the proposed fast algorithm in terms of the performance time as a function of the level in the pyramid. The corresponding plots with the restoration errors are presented in Fig. 7. In these experiments, the STD of the noise is 2. The algorithm becomes faster with an increase in the level of the pyramid, but the quality of restoration rapidly degrades. Figure 8 shows images restored by the fast algorithm with five observed images for the following pyramid levels: $d =$ 1, 2, 3, 4, 5, and 6. It should be noted that good results of restoration are reached only at the first levels, because clear artifacts (vertical or horizontal lines) are not seen and the processing time is significantly smaller than that of the proposed method without pyramidal decomposition, which was described in Section 1.1.

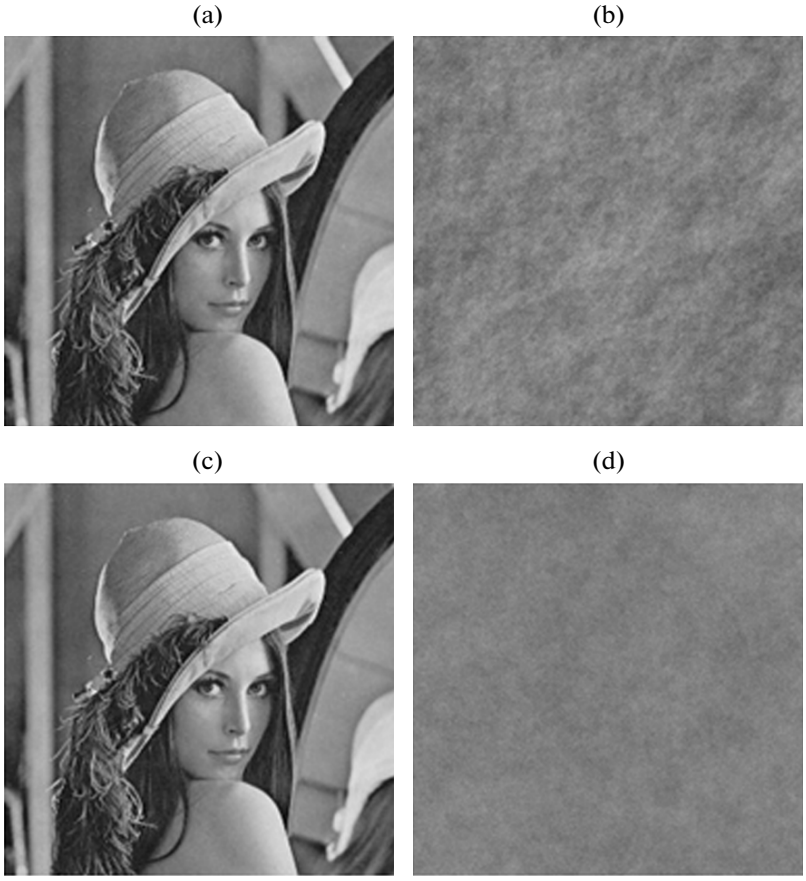

Fig. 5. Results of restoration by the proposed method for an additive interference: (a) the image restored using three images, (b) the enhanced difference between the original image and the image restored with the use of three images, (c) the image restored using five images, and (d) the enhanced difference between the original image and the image restored with the use of five images.

3.2. Multiplicative Inhomogeneous Interferences

An example of multiplicative inhomogeneous interferences is nonuniform illumination of the scene. In this case, the observed image of the scene is formed depending on the light source and the type of the surface. In our experiments, we used a Lambert surface (obeying the Lambert law of reflection of light), i.e., light is reflected from the surface uniformly in all directions. The reflectance function [20, 21] can be written as

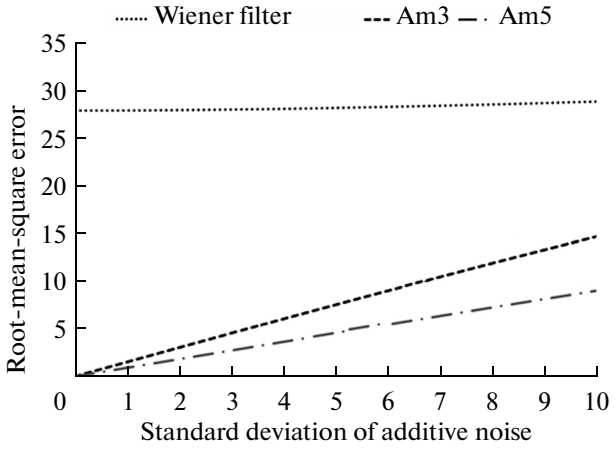

Fig. 6. Results of restoration for an additive interference: RMSE vs. the standard deviation of additive noise.

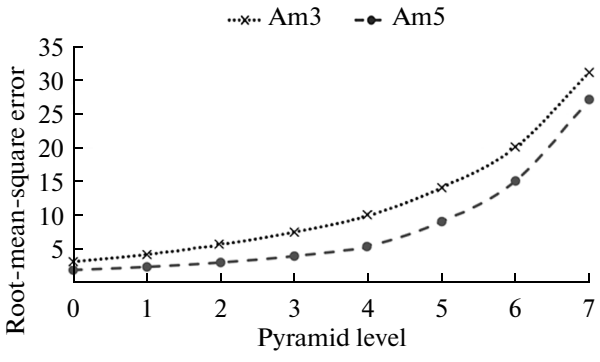

Fig. 7. Results of restoration for an additive interference: RMSE vs. the pyramid level.

Table 1. Time of restoration of the entire image by the proposed fast algorithm vs. the pyramid level for additive interference

Pyramid level	Size of small images	Number of small images	Number of iterations per small image		Time for restoration of the entire image, s	
			3 images	5 images	3 images	5 images
0	256 × 256	1	1084	1060	42.44	42.44
1	128 × 128	4	540	549	10.32	10.30
2	64 × 64	16	280	278	2.95	2.94
3	32 × 32	64	140	140	0.83	0.83
4	16 × 16	256	70	69	0.33	0.33
5	8 × 8	1024	34	32	0.18	0.18
6	4 × 4	4096	10	10	0.15	0.15
7	2 × 2	16384	3	3	0.15	0.15

$$I(p_0, q_0) = \cos\left\{\frac{\pi}{2} - \arctan\left[\frac{r}{\cos(\tau)[(r\tan(\tau)\cos(\alpha) - p_0)^2 + (r\tan(\tau)\sin(\alpha) - q_0)^2]^{1/2}}\right]\right\},$$

where τ is the slant angle, α is the tilt angle, and r is the distance from the point source of light to the surface. These parameters completely describe the position of the point source of light relative to the origin of coordinates, as shown in Fig. 9. In our experiments, $\tau = 5°$, $\alpha = 245°$, and $r = 0.3$. The illuminance function in the range [0.1, 1] is shown in Fig. 10a. Figures 10b and 10c show the original and distorted images, respectively. Additionally, the observed image contains additive white noise with zero mean and an STD of 1. Figures 11a and 11c show the images restored with the use of three and five observed images, respectively. Figures 11b and 11d show the enhanced differences between the original image and the images restored with the use of three and five observed images, respectively. As was expected, the algorithm with five images provides slightly better quality of restoration. Figure 12 shows the results of image restoration in terms of the RMSE for three observed images (Mm3), for five observed images (Mm5), and for the Wiener filtering versus the STD of the additive input noise. It should be noted that the algorithm with five images restores the image significantly better than the Wiener filter with known parameters. The algorithm with three images is applicable only in the cases of small STD of the additive input noise.

Now let us present the results of operation of the fast algorithm applied to this multiplicative model. Table 2 presents the results of restoration by the proposed fast algorithm from the viewpoint of the performance time as a function of the level of the pyramid.

The corresponding plots with restoration errors of are presented in Fig. 13. In these experiments, the STD of the noise is 1. The behavior of the algorithm is similar to its behavior in the case of the additive model: the algorithm becomes faster with an increase in the level of the pyramid but the quality of restoration rapidly degrades. Figure 14 shows images restored by the fast algorithm with three and five observed images for the following levels of the pyramid: $d = 1, 2, 3, 4, 5$, and 6. Note that good results of restoration are reached only at first levels of the pyramid, because clear artifacts (vertical and horizontal lines) are not seen and the processing time is significantly smaller than that of the method (without the pyramidal decomposition) described in Section 1.2.

Fig. 8. Results of restoration for the additive model with the use of images for different levels of the pyramidal decomposition: d = (a) 1, (b) 2, (c) 3, (d) 4, (e) 5, and (f) 6.

3.3. Robustness to the Errors in Positions of Sensor Elements

Finally, let us test the tolerance of the proposed methods to small errors in the positions of the sensor elements of the multi-element array during microscanning. Suppose that each sensor element introduces a random positioning error during the input of the observed images (due to a production defect or a positioning error occurring during the input of the image). The positioning error of each element is an independent random variable with a uniform distribution in the interval [–0.5, 0.5]. Figures 15 and 16 show the robustness on image restoration by means of the proposed method with three observed images for the additive and multiplicative models, respectively. It should be noted that the method is robust to inexact positioning of the array receiver in the process of microscanning.

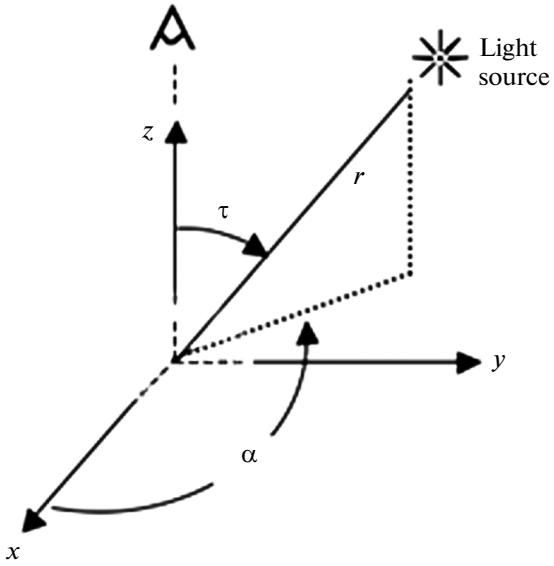

Fig. 9. Geometry of the illumination model.

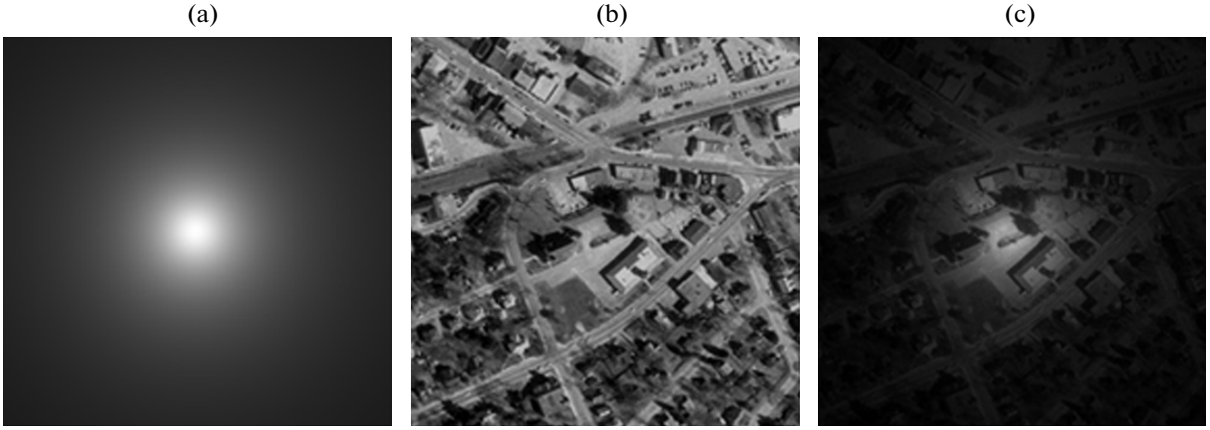

Fig. 10. (a) Function of nonuniform illumination with $\tau = 5°$, $\alpha = 245°$, and $r = 0.3$: (b) the original image; (c) the image distorted by nonuniform illumination and a white noise with a standard deviation of 1.

Table 2. Time of restoration of the entire image by the proposed fast algorithm vs. the pyramid level for a multiplicative interference

Pyramid level	Size of small images	Number of small images	Number of iterations per small image		Time for restoration of the entire image, s	
			3 images	5 images	3 images	5 images
0	256 × 256	1	1069	1060	42.98	42.93
1	128 × 128	4	540	538	10.31	10.30
2	64 × 64	16	274	271	2.95	2.94
3	32 × 32	64	140	137	0.83	0.83
4	16 × 16	256	69	68	0.34	0.34
5	8 × 8	1024	33	32	0.21	0.21
6	4 × 4	4096	10	10	0.17	0.17
7	2 × 2	16384	3	3	0.17	0.17

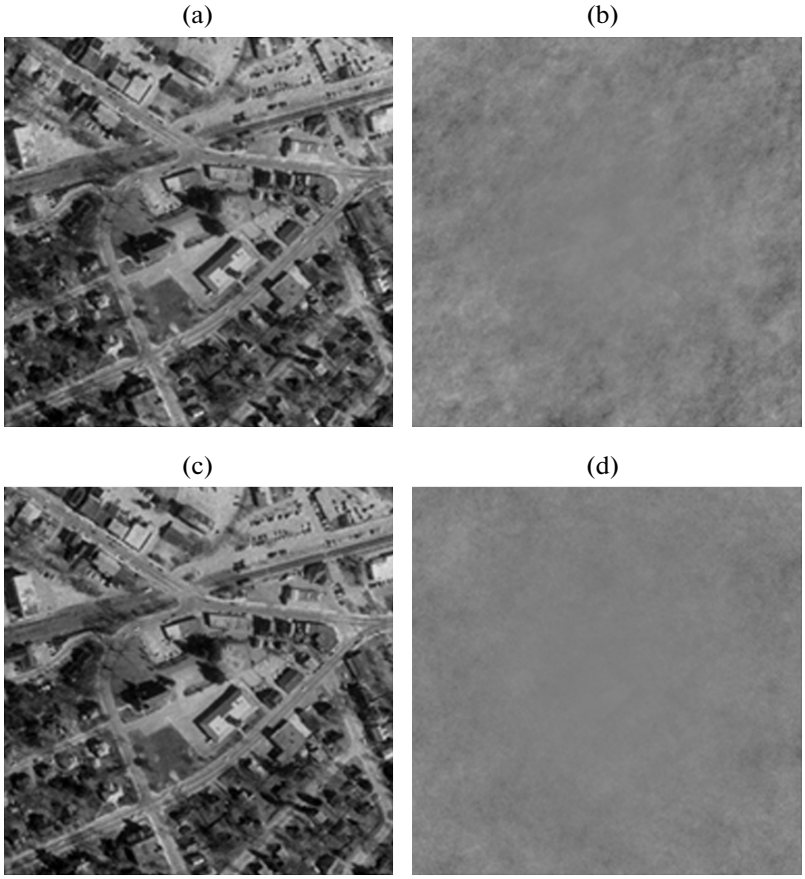

Fig. 11. Results of restoration by the proposed method for a multiplicative interference: (a) the image restored using three images, (b) the enhanced difference between the original image and the image restored with the use of three images, (c) the image restored using five images, and (d) the enhanced difference between the original image and the image restored with the use of five images.

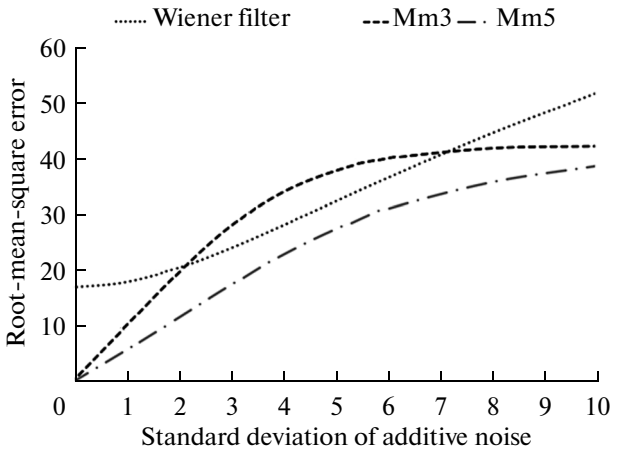

Fig. 12. Results of restoration for a multiplicative interference: RMSE vs. the standard deviation of the additive noise.

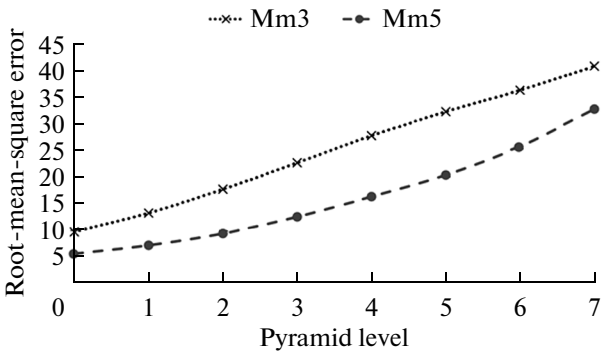

Fig. 13. Results of restoration for a multiplicative interference: RMSE vs. the pyramid level.

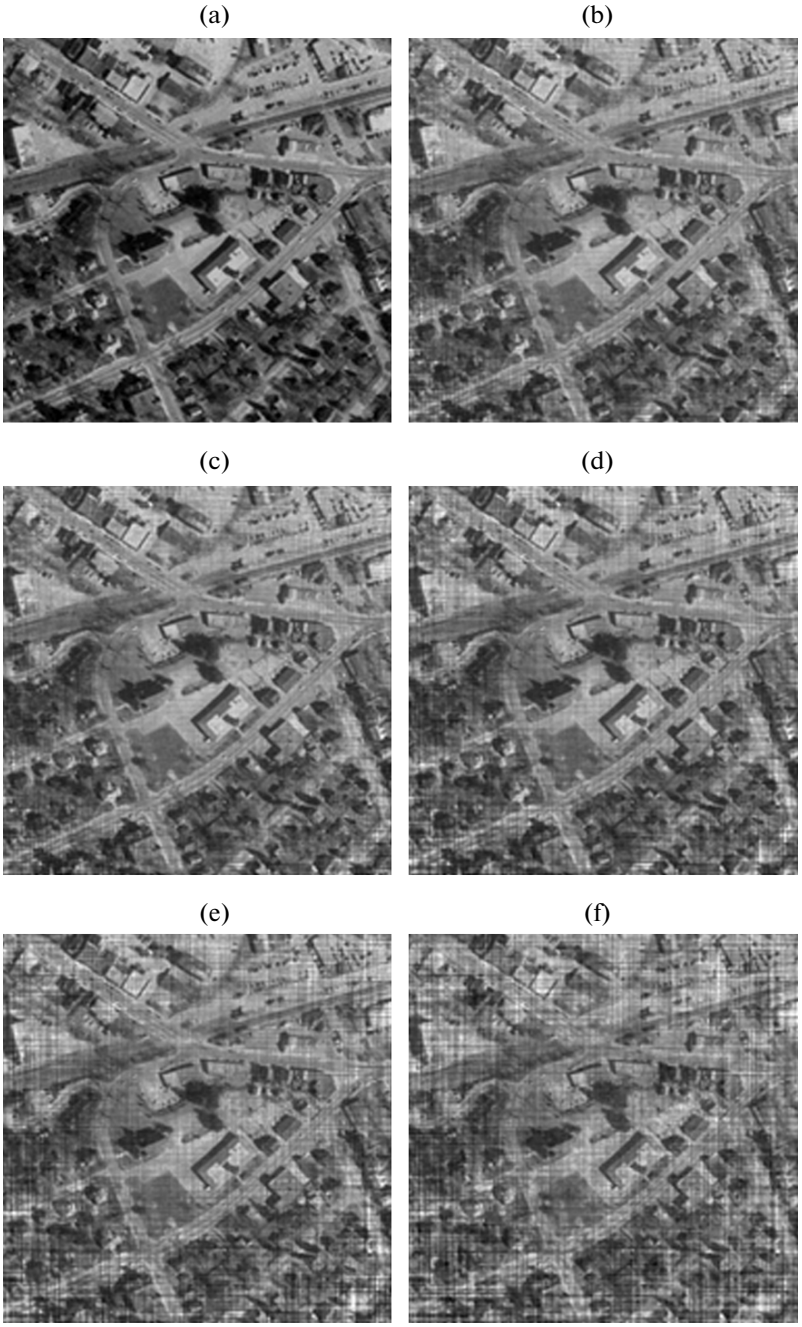

Fig. 14. Results of restoration for the multiplicative model with the use of images for different levels of the pyramidal decomposition: d = (a) 1, (b) 2, (c) 3, (d) 4, (e) 5, and (f) 6.

CONCLUSIONS

In this paper, we have proposed methods for restoration of images distorted by additive and multiplicative interferences. Using several observed images obtained with the use of a multi-element microscanning imaging system, we have derived an explicit system of linear equations for the additive and multiplicative models of distortion. The reconstructed image is a result of solution of the system of linear equations. Since the dimension of the system is very high, the proposed method has a high computational complexity. For solution of this problem, a fast algorithm based on the pyramidal decomposition of images has been proposed. By means of computer simulation, operation of the proposed methods has been demonstrated

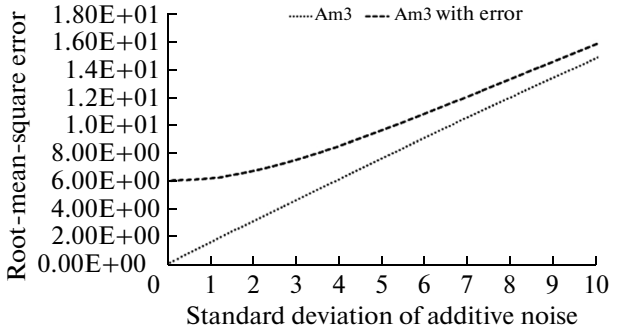

Fig. 15. Results of restoration for an additive interference with subpixel sensors' positioning errors: RMSE vs. the standard deviation of additive noise.

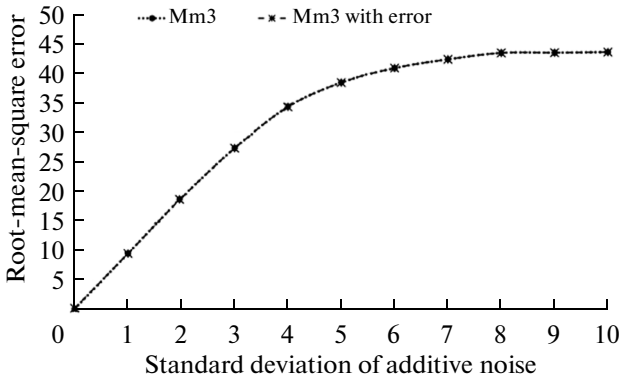

Fig. 16. Results of restoration for a multiplicative interference with subpixel sensors' positioning errors: RMSE vs. the standard deviation of additive noise.

in terms of the accuracy of restoration, performance time, and robustness to sensors' positioning errors in multi-element array sensors.

ACKNOWLEDGMENTS

This work was supported by the CONACYT (grant 157211) and the Ministry of Education and Science (grant 2.1766.2014K).

REFERENCES

1. A. C. Bovik, *Handbook of Image and Video Processing* (Academic, Orlando, 2005).
2. R. C. González and R. E. Woods, *Digital Image Processing* (Prentice Hall, Upper Saddle River, 2008).
3. A. K. Jain, *Fundamentals of Digital Image Processing* (Prentice Hall, Englewood Cliffs, 1988).
4. S. G. Narasimhan and S. K. Nayar, "Vision and the atmosphere", Int. J. Comp. Vision, No. 3, 233–254 (2002).
5. N. Hautiere and D. Aubert, "Contrast restoration of foggy images through use of an onboard camera," in *Proc. IEEE Conf. Intell. Transp. Syst., 2003* (IEEE, New York, 2003), pp. 1090–1090 (2005).
6. S. G. Narasimhan and S. K. Nayar, "Contrast restoration of weather degraded images," IEEE Trans. Pattern. Anal. Mach. Intell., **25**, 713–724 (2003).
7. B. M. Ratliff, M. M. Hayat, and R. C. Hardie, "An algebraic algorithm for nonuniformity correction in focal-plane arrays," J. Opt. Soc. Am. A **19**, 1737–1747 (2002).
8. A. Ferrero, J. Alda, J. Campos, J. M. Lopez-Alonso, and A. Pons, "Principal components analysis of the photoresponse nonuniformity of a matrix detector," Appl. Opt. **46**, 9–17 (2007).
9. P. García-Martínez, M. Tejera, C. Ferreira, D. Lefebvre, and H. Arsenault, "Optical implementation of the weighted sliced orthogonal nonlinear generalized correlation for nonuniform illumination conditions," Appl. Opt. **41**, 6867–6874 (2007).
10. D. Kundur and D. Hatzinakos, "Blind image deconvolution: An algorithmic approach to practical image restoration," IEEE Signal Process. Mag. **13** (3), 43–64 (1996).
11. S. Uma and S. Annadurai, "A review-restoration approaches," ICGST Int. J. Grap. Vision. Im. Process. **8**, 23–35 (2005).
12. M. Banham and A. Katsaggelos, "Digital image restoration," IEEE Signal Process. Mag., **14**, 24–41 (1997).
13. J. L. Lopéz-Martínez and V. Kober, "Image restoration based on camera microscanning," Proc. SPIE: Appl. Digital Image Process. XXXI **7073**, 707322 (2008).
14. J. L. Lopéz-Martínez and V. Kober, "Fast image restoration algorithm based on camera microscanning," Proc. SPIE: Appl. Digital Image Process. XXXII **7443**, 744310 (2009).
15. J. L. Lopéz-Martínez and V. Kober, "Image restoration of nonuniformly illuminated images with camera microscanning," Proc. SPIE: Appl. Digital Image Process. XXXIII **7798**, 77982D (2010).
16. J. L. Lopéz-Martínez, V. Kober, and I. A. Ovseyevich, "Image restoration based on camera microscanning," Pattern Recogn. Image Analysis **20**, 370–375 (2010).
17. J. Shi, S. E. Reichenbach, and J. D. Howe, "Small-kernel superresolution methods for microscanning imaging systems," Appl. Opt. **45**, 1203–1214 (2006).
18. G. Golub and C. Van Loan, *Matrix Computations* (Johns Hopkins Univ. Press, Baltimore, 1996).
19. V. Kober, M. Mozero, and J. Alvarez-Borrego, "Nonlinear filters with spatially connected neighborhoods," Opt. Eng. **40**, 971–983 (2001).
20. B. K. P. Horn and R. W. Sjoberg, "Calculating the reflectance map," Appl. Opt. **18**, 1770–1779 (1979).
21. V. H. Diaz-Ramirez and V. Kober, "Target recognition under nonuniform illumination conditions," Appl. Opt. **48**, 1408–1418 (2009).

Translated by E. Chernokozhin